Available online at www.sciencedirect.com
SCIENCE DIRECT®
International Journal of Thermal Sciences 45 (2006) 697–705
International Journal of Thermal Sciences
www.elsevier.com/locate/ijts

Rayleigh–Bénard convection in two-dimensional arbitrary finite domains

H.M. Park *, Y.M. Heo

Department of Chemical Engineering, Sogang University, Seoul, South Korea

Received 24 September 2004; received in revised form 15 March 2005; accepted 3 October 2005

Available online 14 November 2005

Abstract

In the present work, we consider the linear and nonlinear hydrodynamic stability problems of two-dimensional Rayleigh–Bénard convection in arbitrary finite domains. The effects of the domain shapes on the critical Rayleigh number and convection pattern are investigated by means of a linear stability analysis employing a Chebyshev pseudospectral method. An extension of the present technique to nonlinear stability analysis allows derivation of the Landau equation for arbitrary finite domains. The results of nonlinear stability analysis are confirmed by comparison with numerical solution of the Boussinesq set. The results of the present investigation may be exploited to enhance or suppress thermal convection by varying system domain.

Keywords: Nonlinear hydrodynamic stability; Arbitrary finite domains

1. Introduction

The Rayleigh–Bénard convection has been extensively studied experimentally and theoretically because of its frequent occurrence in various fields of science and engineering. A full account of the linearized theory is given in Chandrasekhar [1] and Drazin and Reid [2]. Although the linear theory determines the critical Rayleigh number and wavenumber, it does not predicts the intensity of convection for a given Rayleigh number. The nonlinear stability analysis based on perturbation methods yield the Landau equation which can answer this question. The first work in this direction was done by Malkus and Veronis [3] and generalized by Schlüter et al. [4] and many others.

All these analyses assume that the flow and temperature fields are periodic in the horizontal directions and seek normal mode solutions so that the resulting equation for the hydrodynamic stability analysis become one-dimensional, which can be solved even analytically. Later, to make the analysis more compatible with experiments, some investigators try to consider the effects of lateral walls on the flow pattern and size of convection cells numerically as well as theoretically. Davis [5] was the first investigator to study the linear hydrodynamic stability of the Rayleigh–Bénard convection in a fully confined domain numerically. Reddy and Voyè [6] and van de Vooren and Dijkstra [7] employed a finite element method to analyze linear convective instability in finite domains. Thermal convection in cylindrical containers has been investigated by Charlson and Sani [8] and Crespo del Arco and Bontoux [9]. Recently, Park and Ryu [10] derived a Landau equation for the Rayleigh–Bénard convection in confined finite domains and compared its predictions with the results of exact numerical solution of the Boussinesq equation. There have been also other attempts to consider the effects of confining sidewalls employing multi-scale perturbation theory. In a seminal paper Segel [11] investigated the consequences of the presence of vertical lateral walls in a rectangular container on the onset and the amplitude of convection and derived a Ginzburg–Landau type equation. This kind of analysis was later employed by other investigators [12] to study the effect of a small heat transfer through the sidewalls, which makes the onset of convection an imperfect bifurcation. The Ginzburg–Landau equation derived through the multi-scale perturbation method has been extensively employed in the study of pattern formation in the Rayleigh–Bénard convection [13]. Nonlinear analysis in a vertical cylinder has been done by Hardin and Sani [14]. All these analyses until now are related with the Rayleigh–Bénard convection in rectangular, cylindrical or spherical domains where the governing equations are separable in the corresponding coordinate system.

In the present work, we study the Rayleigh–Bénard convection in finite arbitrary shaped domains. Obviously, the inten-

* Corresponding author.
E-mail address: hmpark@ccs.sogang.ac.kr (H.M. Park).

1290-0729/$ – see front matter
doi:10.1016/j.ijthermalsci.2005.10.002

sity of thermal convection and the critical Rayleigh number depend crucially on the shapes of the domain. Therefore the shape of the convection domain may be considered as an important control parameter in adjusting convection. For example, a judicious design of the sidewall shapes can suppress or enhance the natural convection in the vessel. Until now, there were no appropriate analysis tools for this interesting problems of hydrodynamic stability. But recently we proposed a method of linear and nonlinear hydrodynamic stability analysis in confined domains with nonslip walls [10] by exploiting the Chebyshev pseudospectral method [15]. In the present investigation, we extend this technique to solve the linear and nonlinear hydrodynamic stability problems of the Rayleigh–Bénard convection in two-dimensional finite domains of various shapes. After transforming the irregular physical domains to a square computational domain, we reformulate the Boussinesq equation using the stream function so that the incompressibility condition is imposed exactly. The discretization through the Chebyshev pseudospectral method yields algebraic eigenvalue problems which can be solved to find the eigenvalues and eigenvectors needed in the linear stability analysis. The critical eigenvalue and eigenfunction are further adopted in the nonlinear stability analysis employing the power series method [4]. The results of the nonlinear stability analysis are confirmed by comparison with the numerical solution of the Navier–Stokes equation with the Boussinesq approximation. In various industrial processes, it is desirable to suppress thermal convection as in the Czochralski process of semiconductor manufacturing. In other cases, thermal convection improves the product quality by inducting mixing. The present investigation may show some clues of geometrically controlling thermal convection. At the onset of thermal convection, the convergence rate of any numerical scheme is very slow, which causes a tremendous amount of computer time. The nonlinear stability analysis of the present work is an economic way of obtaining convection patterns near the critical Rayleigh number.

2. System and governing equations

We consider an incompressible fluid with the Boussinesq approximation in a two-dimensional domain whose bottom is maintained at a higher temperature than the top. The shapes of the domain are such that the top and bottom are flat, whereas the sidewalls are of arbitrary shapes. We define the dimensionless variables by the following equations, where the superscript asterisk is used to denote the dimensional quantities:

$$x = \frac{x^*}{d_y}, \qquad y = \frac{y^*}{d_y}, \qquad t = \frac{\kappa t^*}{d_y^2}, \qquad \mathbf{v} = \frac{d\mathbf{v}^*}{\kappa}$$
$$T = \frac{T^* - T^*_{\text{cold}}}{T^*_{\text{hot}} - T^*_{\text{cold}}}, \qquad P' = \frac{d^2 P^*}{\rho \kappa^2} \tag{1}$$

where T^*_{hot} is the hot bottom temperature, T^*_{cold} is the cold top temperature, t^* is time, $\mathbf{v}^*$ is the velocity field, P^* is the pressure field, κ is the thermal diffusivity, ρ is the density, d_y is the characteristic depth of the domain. In consistent with the Boussinesq approximation, we regard the physical properties of the fluid constant except the density in the body force term, which is represented as a function of temperature. For later purpose, we define the dimensionless group R the Rayleigh number, and Pr the Prandtl number as follows:

$$R = \alpha g \frac{(T^*_{\text{hot}} - T^*_{\text{cold}}) d_y^3}{\kappa \nu}, \qquad Pr = \frac{\nu}{\kappa} \tag{2}$$

where α is the thermal expansion coefficient, g is the gravitational constant and ν is the kinematic viscosity. In the present investigation, we take $Pr = 0.72$. With isothermal sidewalls, there exists a critical Rayleigh number for the domains under consideration below which there is no fluid motion. The basic state or the conduction state is denoted by $(\mathbf{v}^s, T^s)$.

Then relevant boundary conditions for the T^s field are; $T^s = 1.0$ at the bottom, $T^s = 0.0$ at the top boundary and Dirichlet temperature boundary condition on the sidewalls, where temperature varies linearly with respect to height. The deviational temperature Θ is defined by

$$\Theta = T - T^s \tag{3}$$

In terms of the streamfunction ψ and the deviational temperature, the governing equations for the two-dimensional system may be rewritten as [1]:

$$\frac{\partial}{\partial t}\left(\nabla^2 \psi\right) + J\left(\nabla^2 \psi, \psi\right) = Pr \nabla^4 \psi - R\,Pr \frac{\partial \Theta}{\partial x} - R\,Pr \frac{\partial T^s}{\partial x} \tag{4}$$

$$\frac{\partial \Theta}{\partial t} + J(\Theta, \psi) = \nabla^2 \Theta + \frac{\partial \psi}{\partial x}\frac{\partial T^s}{\partial y} - \frac{\partial \psi}{\partial y}\frac{\partial T^s}{\partial x} \tag{5}$$

where the Jacobian J is defined as

$$J(f, g) = \begin{vmatrix} \frac{\partial f}{\partial x} & \frac{\partial f}{\partial y} \\ \frac{\partial g}{\partial x} & \frac{\partial g}{\partial y} \end{vmatrix} \tag{6}$$

The boundary conditions are such that stream function and its normal derivative, ψ and $\frac{\partial \psi}{\partial n}$, and Θ are zero at the walls. In Eqs. (12) and (13), $\frac{\partial T^s}{\partial x} \equiv 0$ for the condition of isothermal sidewall temperature which is varying linearly with respect to y. The analysis shall be done in a fixed square computational domain (ξ, η) rather than in the irregular physical domain.

The transformation between the physical domain (x, y) and the computational domain (ξ, η) is performed by means of the following set of elliptic equations [16]:

$$(\sqrt{g})^2 g^{11} \frac{\partial^2 x}{\partial \xi^2} + 2(\sqrt{g})^2 g^{12} \frac{\partial^2 x}{\partial \xi \partial \eta} + (\sqrt{g})^2 g^{22} \frac{\partial^2 x}{\partial \eta^2} = -(\sqrt{g})^2 \left(P \frac{\partial x}{\partial \xi} + Q \frac{\partial x}{\partial \eta} \right) \tag{7}$$

$$(\sqrt{g})^2 g^{11} \frac{\partial^2 y}{\partial \xi^2} + 2(\sqrt{g})^2 g^{12} \frac{\partial^2 y}{\partial \xi \partial \eta} + (\sqrt{g})^2 g^{22} \frac{\partial^2 y}{\partial \eta^2} = -(\sqrt{g})^2 \left(P \frac{\partial y}{\partial \xi} + Q \frac{\partial y}{\partial \eta} \right) \tag{8}$$

The variables P and Q in Eqs. (7)–(8) are adjusted such that the grids intersect the boundary orthogonally. As a result, the boundary conditions for Eqs. (4)–(5) in the computational domain are given by:

$$\xi = \pm 1; \quad \psi = 0, \ \frac{\partial \psi}{\partial \xi} = 0, \ \Theta = 0 \tag{9}$$

$$\eta = \pm 1; \quad \psi = 0, \ \frac{\partial \psi}{\partial \eta} = 0, \ \Theta = 0 \tag{10}$$

3. Linear stability analysis

Assuming

$$\psi(\xi, \eta) = e^{st}\varphi(\xi, \eta) \tag{11}$$

$$\Theta(\xi, \eta) = e^{st}\theta(\xi, \eta) \tag{12}$$

Eqs. (4)–(5) become a differential eigenvalue problem, where s is the eigenvalue determining the stability of the basic state. The boundary conditions for φ and θ are the same as those for ψ and Θ. As previously [10], the Chebyshev pseudospectral method [13] is employed to convert the differential eigenvalue problem to an algebraic eigenvalue problem after imposing the relevant boundary conditions. Using the Chebyshev pseudospectral method, we can approximate differentiations of a function by matrix multiplications as follows:

$$\frac{\partial^q f}{\partial x^q}(x_i, y_j) = \sum_{l=1}^{NX+1} \widehat{GX}_{i,l}^{(q)} f_{l,j} \tag{13}$$

$$\frac{\partial^q f}{\partial y^q}(x_i, y_j) = \sum_{l=1}^{NY+1} \widehat{GY}_{j,l}^{(q)} f_{i,l} \quad (1 \leqslant i \leqslant NX+1, \ 1 \leqslant j \leqslant NY+1) \tag{14}$$

where (x_i, y_j) is the Chebyshev collocation point [10], the grid variable $f_{l,j}$ is the value of $f(\xi, \eta)$ at the collocation point (ξ_l, η_j), $NX+1$ is the total number of grids in the ξ-direction, $NY+1$ is that in the η-direction. The matrices $\widehat{GX}_{i,l}^{(q)}$ and $\widehat{GY}_{j,l}^{(q)}$ have been derived in Ref. [10]. For the variable φ, we impose two separate boundary conditions on each bounding wall. Therefore, we can remove the boundary grid values and the outermost internal grid values of φ in terms of the remaining internal grid values. For example, the boundary conditions (9) for φ yields [10]

$$\varphi_{1,j} = 0; \quad \varphi_{NX+1,j} = 0 \ (1 \leqslant j \leqslant NY+1) \tag{15}$$

$$\sum_{m=1}^{NX+1} \widehat{GX}_{1,m}^{(1)} \varphi_{m,j} = 0$$

$$\sum_{m=1}^{NX+1} \widehat{GX}_{NX+1,m}^{(1)} \varphi_{m,j} = 0 \quad (1 \leqslant j \leqslant NY+1) \tag{16}$$

Solving Eqs. (15)–(16) simultaneously, we can express the outermost internal grid values in terms of the remaining internal grid values [10]:

$$\varphi_{2,j} = \sum_{m=3}^{NX-1} a_m \varphi_{m,j}$$

$$\varphi_{NX,j} = \sum_{m=3}^{NX-1} b_m \varphi_{m,j} \quad (1 \leqslant j \leqslant NY+1) \tag{17}$$

where

$$a_m \equiv \frac{\widehat{GX}_{1,NX}^{(1)} \widehat{GX}_{NX+1,m}^{(1)} - \widehat{GX}_{NX+1,NX}^{(1)} \widehat{GX}_{1,m}^{(1)}}{\widehat{GX}_{1,2}^{(1)} \widehat{GX}_{NX+1,NX}^{(1)} - \widehat{GX}_{1,NX}^{(1)} \widehat{GX}_{NX+1,2}^{(1)}} \tag{18}$$

$$b_m \equiv \frac{\widehat{GX}_{NX+1,2}^{(1)} \widehat{GX}_{1,m}^{(1)} - \widehat{GX}_{1,2}^{(1)} \widehat{GX}_{NX+1,m}^{(1)}}{\widehat{GX}_{1,2}^{(1)} \widehat{GX}_{NX+1,NX}^{(1)} - \widehat{GX}_{1,NX}^{(1)} \widehat{GX}_{NX+1,2}^{(1)}} \tag{19}$$

In a similar manner, the outermost internal grid values $\varphi_{i,2}$ and $\varphi_{i,NY}$ can be represented in terms of the remaining internal grid values [10]. Therefore, the unknown grid values to be determined in the resulting algebraic eigenvalue problem is

$$\mathbf{x}^{\mathrm{T}} = (\varphi_{3,3}, \varphi_{4,3}, \ldots, \varphi_{NX-1,3}, \varphi_{3,4}, \ldots, \varphi_{NX-1,NY-1}, \theta_{2,2}, \theta_{3,2}, \ldots, \theta_{NX,NY}) \tag{20}$$

The resulting algebraic eigenvalue problem may be written as

$$\boldsymbol{\alpha} \cdot \mathbf{x} = s\boldsymbol{\beta} \cdot \mathbf{x} \tag{21}$$

where the matrices $\boldsymbol{\alpha}$ and $\boldsymbol{\beta}$ are constructed by discretizing Eqs. (4)–(5) after transforming to the computational domain and substituting Eqs. (11)–(12). The basic state becomes unstable and convective flow sets in when the real part of s becomes positive. The critical Rayleigh number is defined as the smallest Rayleigh number when the largest real part of s is zero. For Rayleigh–Bénard convection, when the largest real part of s is zero, the corresponding imaginary part of s is always zero; i.e., the exchange of stabilities is valid [1,2]. The matrix eigenvalue problem, Eq. (21), is solved using a standard package such as the IMSL. We adopt a (30×15) grids with double precision arithmetic. Employment of a finer grid system (40×20) changes the critical Rayleigh number less than 0.01%. The sufficiency of the grid numbers for the similar systems is also confirmed in the previous works [10].

4. Dependence of the critical Rayleigh number and eigenfunctions on the shapes of the domain

Before investigating the effects of boundary shapes on the Rayleigh–Bénard convection, we examine the critical Rayleigh number for rectangular finite domains with various box aspect ratio d_x/d_y, where d_x is the width and d_y is the depth of the box, for the case of adiabatic sidewalls $\frac{\partial \Theta}{\partial x} = 0$ and zero deviatoric temperature sidewalls $\Theta = 0$, respectively. For brevity, we call the latter case the isothermal sidewall.

In our previous work [10], we adopt the half depth of the domain as the characteristic length when converting the governing equations to the dimensionless form. In the present investigation, however, we adopt the depth of the domain as the characteristic length. Therefore the R_a in the present work is eight times as large as that in Ref. [10]. The adiabatic case has been extensively investigated in our previous work [10], and we shall concentrate on the isothermal case in the present investigation. As shown in Fig. 1, the critical Rayleigh number R_c decreases as the aspect ratio increases for both cases. The case of isothermal sidewalls has higher R_c values than that of adiabatic sidewalls, especially for smaller values of the aspect

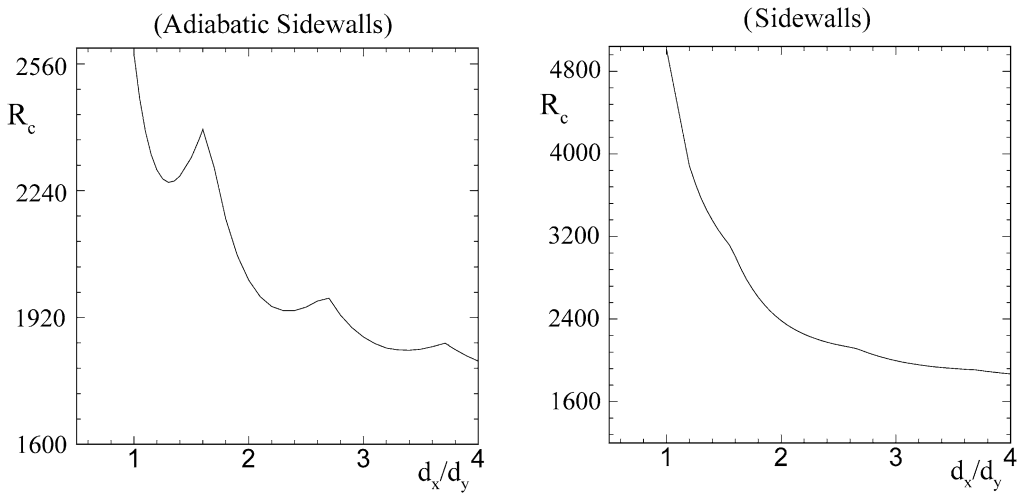

Fig. 1. Critical Rayleigh number versus the aspect ratio.

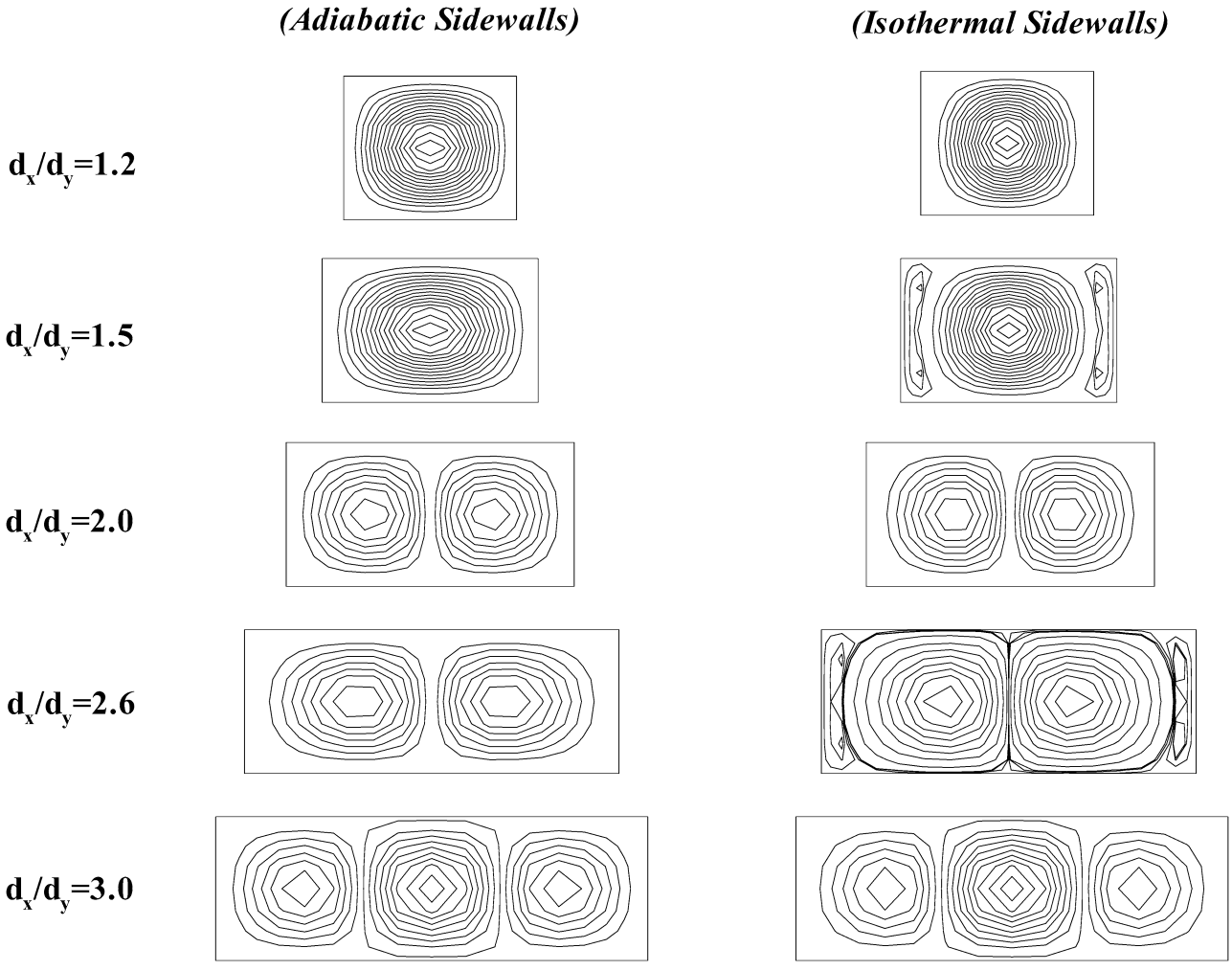

Fig. 2. Temperature perturbation eigenfunction (Θ) at various aspect ratios.

ratio, since there is heat efflux through the sidewalls for the former case. Each curve in Fig. 1 consists of several piecewise continuous smooth curves, each smooth section of the curve corresponding to a particular mode number, i.e., number of convection cells at onset of instability.

The mode number increases discretely as the aspect ratio d_x/d_y increases. For example, the number of convection cells around $d_x/d_y = 2$ is two. It is interesting to note that R_c decreases monotonically with respect to d_x/d_y for the case of isothermal sidewalls, while R_c increases for a short interval of

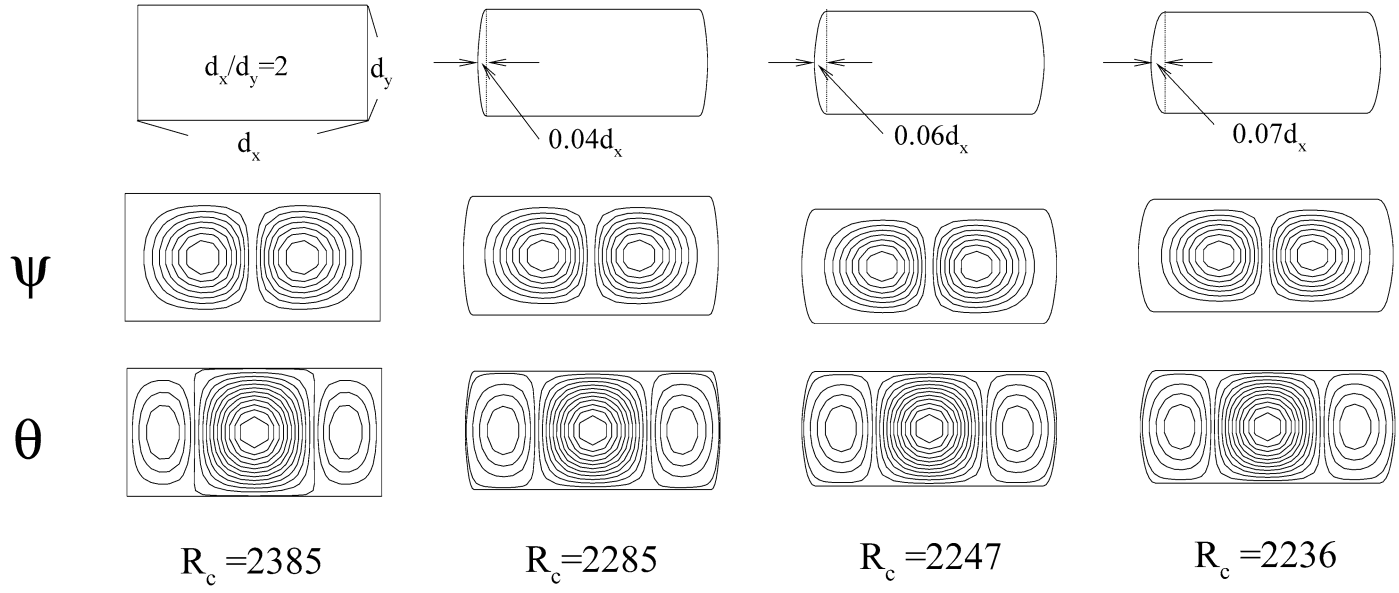

Fig. 3. Three shapes with bulged sidewalls, their critical eigenfunctions, Ψ, Θ, and the critical Rayleigh numbers.

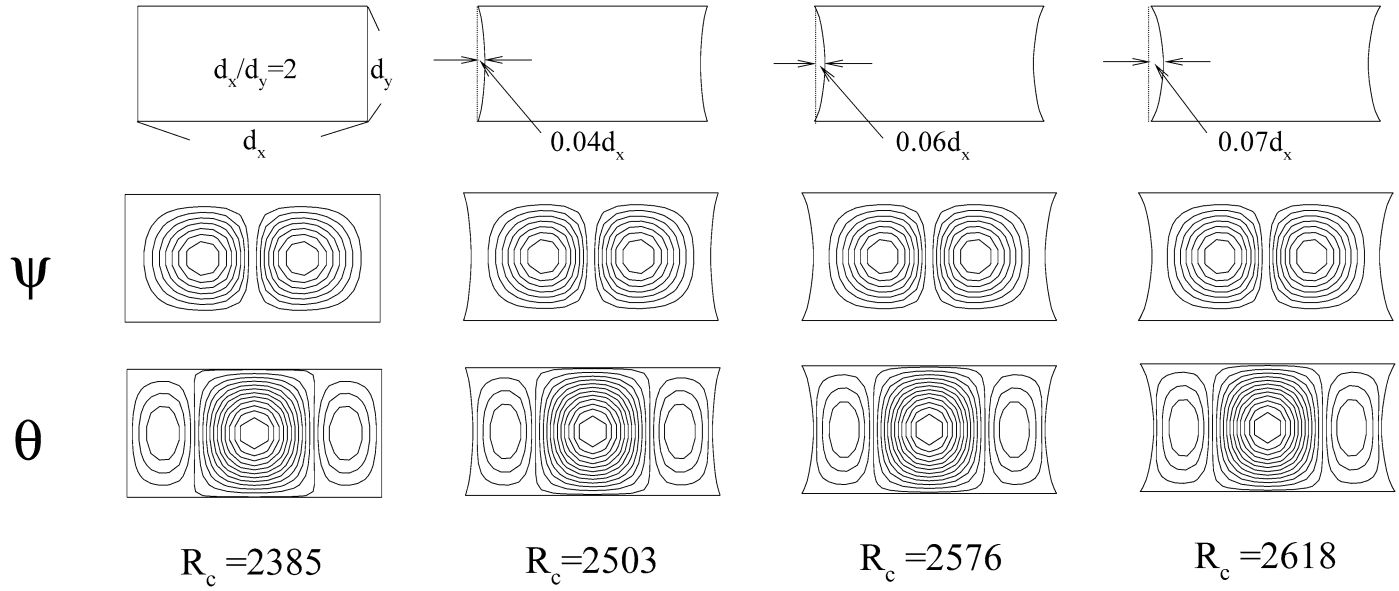

Fig. 4. Domains with inwardly curved sidewalls, their critical eigenfunctions, Ψ, Θ, and the critical Rayleigh numbers.

d_x/d_y before the number of cells increases and then R_c drops again after the cell number increases for the case of adiabatic sidewalls. This difference is caused by the formation of small satellite convection cells near the sidewalls before the number of convection cells increases for the isothermal case. For example, the number of cells increases from one to two around $d_x/d_y \approx 1.65$ as shown in Fig. 1. For the adiabatic case, the R_c increases for $1.3 \leqslant d_x/d_y \leqslant 1.65$ owing to the competition between one-cell mode and two-cell mode. On the other hand, small satellite cells begin to appear near the sidewalls for this range of aspect ratio in the isothermal case owing to the efflux of heat and, as a result, the R_c does not increase before switching to the two-cell mode at $d_x/d_y \approx 1.65$. Fig. 2 shows the convection patterns at various aspect ratios for the case of adiabatic sidewalls and isothermal sidewalls at various aspect ratios, where the formation of satellite cells is depicted clearly for the case of isothermal sidewalls. Now, we move to the investigation on the effects of the shape of domain on the critical Rayleigh number for the case of isothermal sidewalls. First consideration is the three shapes depicted in Fig. 3, which have progressively larger bulged sidewalls with $d_x/d_y = 2.0$. Also shown in the same figure are the critical temperature eigenfunctions Θ as well as the corresponding critical Rayleigh numbers. As expected from the results of Fig. 1, the critical Rayleigh number decreases as the sidewall bulge becomes larger, which has a similar effect to the increased aspect ratio. Next consideration is the domains with inwardly curved sidewalls as shown in Fig. 4. The distortion of the sidewalls of domains in Fig. 4 is in opposite direction to that of domains in Fig. 3.

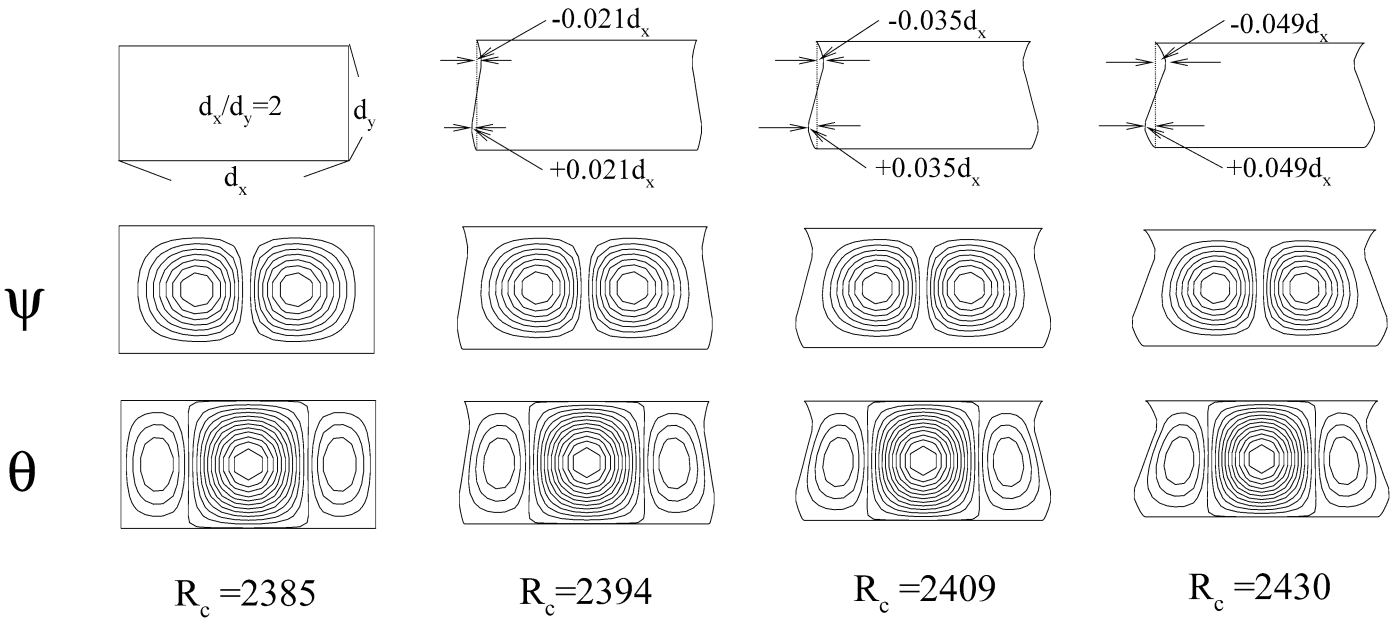

Fig. 5. Shapes having a constant volume (one sinusoidal wavelength).

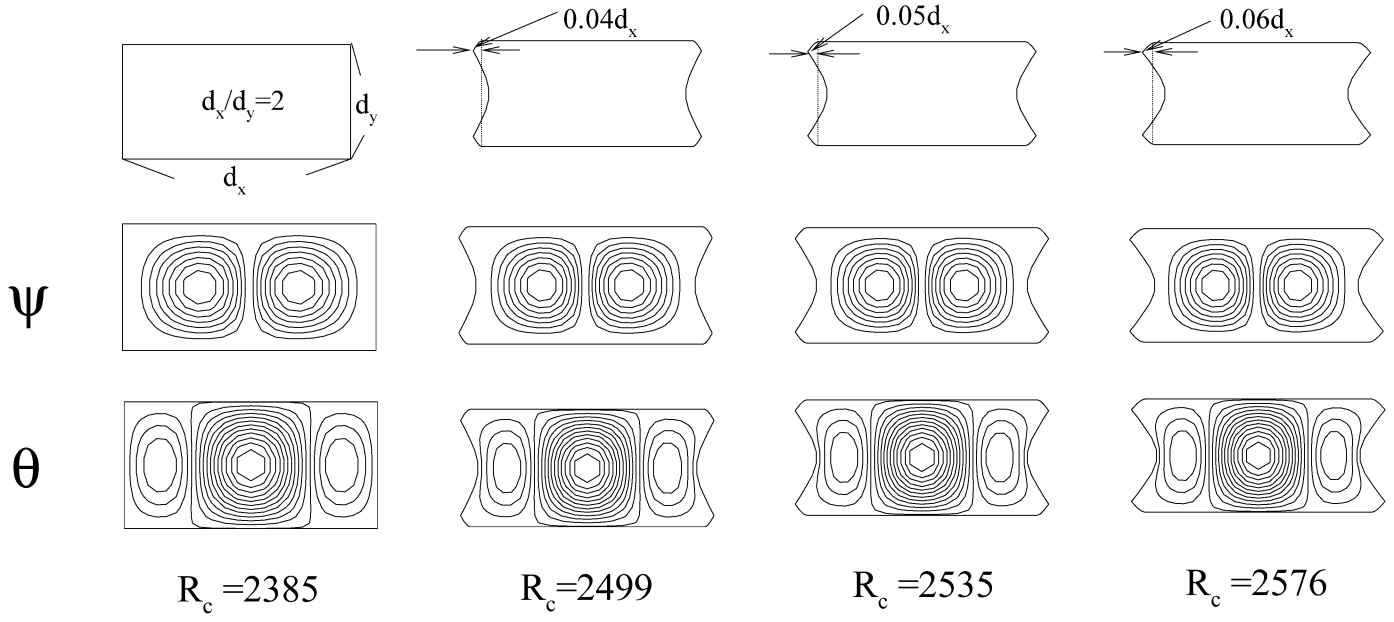

Fig. 6. Shapes having a constant volume (one and a half wavelength).

It is shown that the critical Rayleigh number increases monotonically as the sidewalls distort inwardly, which is tantamount to the decreased aspect ratio. If we imposed adiabatic boundary condition instead of the isothermal one, we might have found a somewhat different trends for certain intervals of the aspect ratio. For example, for the inwardly distorted shapes with the aspect ratio around 2.5, the critical Rayleigh number may decrease as the sidewalls distort inwardly with the adiabatic boundary condition (cf. Fig. 1). But we need a somewhat different technique of stability analysis for the case of curved sidewalls with the adiabatic boundary condition, since there exists nonzero basic flows in this case.

The above two sets of domains have volumes different from that of the rectangular domain, while the heat input into the system through the bottom boundary is the same. To make a fair comparison, we arrange two more sets of domains, depicted in Figs. 5 and 6, each of which has exactly the same volume as the rectangular one. The domains in Figs. 5 and 6 have sinusoidally varying sidewalls. The sidewalls of Fig. 5 have one wavelength, while those of Fig. 6 have one and a half wavelength. It is shown that the sinusoidal distortion hinders thermal convection, thus increasing the critical Rayleigh number. It is also shown that the increase of the critical Rayleigh number is proportional to the amplitude and the frequency of the sinusoidal distortion of the sidewalls.

5. Nonlinear stability analysis

The magnitude of convection intensity can be predicted through a nonlinear stability analysis employing the power series method [4,10]. Since the direct numerical solution of the Navier–Stokes equation with Boussinesq approximation requires a tremendous amount of computer time when the Rayleigh number is near the critical one, the nonlinear stability analysis can be an economical alternative way of obtaining convection patterns near the critical Rayleigh number. Introducing a small perturbation parameter ε, which indicates deviation from the critical state, the variables may be expanded as a power series of ε for a weakly nonlinear state:

$$R = R_c + \varepsilon^2 R_2 + \cdots \tag{22}$$

$$\Theta = \varepsilon\Theta_{(1)} + \varepsilon^2\Theta_{(2)} + \varepsilon^3\Theta_{(3)} + \cdots \tag{23}$$

$$\psi = \varepsilon\psi_{(1)} + \varepsilon^2\psi_{(2)} + \varepsilon^3\psi_{(3)} + \cdots \tag{24}$$

The scaling for the time variable t is such that $\partial/\partial t = \varepsilon^2\partial/\partial\tau$. The term R_1 in (22) is eliminated a priori, since it becomes zero owing to the symmetry in the boundary condition when the solvability condition is imposed. When the disturbance variables defined as above are substituted into the governing equation, we find the following sequence of equations in the computational domain:

O(ε):

$$Pr\frac{1}{\sqrt{g}}\frac{\partial}{\partial\xi^i}\left[\sqrt{g}g^{ij}\frac{\partial}{\partial\xi^j}\left\{\frac{1}{\sqrt{g}}\frac{\partial}{\partial\xi^k}\left(\sqrt{g}g^{kl}\frac{\partial}{\partial\xi^l}\right)\right\}\right]\psi_{(1)} - R_c Pr\,\varepsilon_{ij3}\frac{1}{\sqrt{g}}y_{\xi^j}\frac{\partial}{\partial\xi^i}\Theta_{(1)} = 0 \tag{25}$$

$$\frac{1}{\sqrt{g}}\frac{\partial}{\partial\xi^i}\left(\sqrt{g}g^{ij}\frac{\partial}{\partial\xi^j}\right)\Theta_{(1)} - \frac{1}{2}\varepsilon_{ij3}\frac{1}{\sqrt{g}}y_{\xi^j}\frac{\partial}{\partial\xi^i}\psi_{(1)} = 0 \tag{26}$$

or

$$L\begin{bmatrix}\psi_{(1)}\\ \Theta_{(1)}\end{bmatrix} = 0 \tag{27}$$

where L is a linear operator determined from Eqs. (25) and (26).

O(ε^2):

$$L\begin{bmatrix}\psi_{(2)}\\ \Theta_{(2)}\end{bmatrix} = \begin{bmatrix}J(\nabla^2\psi_{(1)},\psi_{(1)})\\ J(\Theta_{(1)},\psi_{(1)})\end{bmatrix} \tag{28}$$

O(ε^3):

$$L\begin{bmatrix}\psi_{(3)}\\ \Theta_{(3)}\end{bmatrix} = \begin{bmatrix}\frac{\partial}{\partial\tau}\nabla^2\psi_{(1)} + J(\nabla^2\psi_{(1)},\psi_{(2)}) + J(\nabla^2\psi_{(2)},\psi_{(1)}) + R_2 Pr\,\varepsilon_{ij3}\frac{1}{\sqrt{g}}y_{\xi^j}\frac{\Theta_{(1)}}{\partial\xi^i}\\ \frac{\partial\Theta_{(1)}}{\partial\tau} + J(\Theta_{(1)},\psi_{(2)}) + J(\Theta_{(2)},\psi_{(1)})\end{bmatrix} \tag{29}$$

In the above equations, the Jacobian is defined by

$$J(f,g) \equiv \left[\varepsilon_{ij3}\frac{1}{\sqrt{g}}y_{\xi^j}\frac{\partial f}{\partial\xi^i}\right]\left[\varepsilon_{ij3}\frac{1}{\sqrt{g}}x_{\xi^i}\frac{\partial g}{\partial\xi^j}\right] - \left[\varepsilon_{ij3}\frac{1}{\sqrt{g}}x_{\xi^i}\frac{\partial f}{\partial\xi^j}\right]\left[\varepsilon_{ij3}\frac{1}{\sqrt{g}}y_{\xi^j}\frac{\partial g}{\partial\xi^i}\right] \tag{30}$$

and

$$\nabla^2\psi_{(l)} = \frac{1}{\sqrt{g}}\frac{\partial}{\partial\xi^i}\left(\sqrt{g}g^{ij}\frac{\partial\psi_{(l)}}{\partial\xi^j}\right) \quad (l=1,2) \tag{31}$$

Since the grids are generated such that they intersect the boundaries orthogonally, the relevant boundary conditions are given by

$$\xi = \pm 1; \quad \psi_{(l)} = 0,\ \frac{\partial\psi_{(l)}}{\partial\xi} = 0,\ \Theta_{(l)} = 0\ (l=1,2,3) \tag{32}$$

$$\eta = \pm 1; \quad \psi_{(l)} = 0,\ \frac{\partial\psi_{(l)}}{\partial\eta} = 0,\ \Theta_{(l)} = 0\ (l=1,2,3) \tag{33}$$

The perturbation equations for each order may be solved as follows.

(1) *First order* (ε). The first-order equations, Eq. (27), with the relevant boundary conditions are the same as those for the linear stability analysis, Eq. (21), with $s = 0$. Therefore, Eq. (27) may be discretized as

$$\boldsymbol{\alpha}\cdot\mathbf{x}_{(1)} = 0 \tag{34}$$

Here $\boldsymbol{\alpha}$ is the same matrix as defined in Eq. (21) and $\mathbf{x}_{(1)}$ is defined as

$$\mathbf{x}_{(1)} = \left(\psi^{(1)}_{3,3}, \psi^{(1)}_{4,3}, \ldots, \psi^{(1)}_{NX-1,NY-1}, \Theta^{(1)}_{2,2}, \Theta^{(1)}_{3,2}, \ldots, \Theta^{(1)}_{NX,NY}\right)^{\mathrm{T}} \tag{35}$$

The solution of Eq. (35) is the eigenvector of the linear stability equation (Eq. (21)) with zero eigenvalue ($s = 0$). We may write the first-order solution as

$$\mathbf{x}_{(1)} = C\mathbf{x} \tag{36}$$

where $\mathbf{x}$ is given by Eq. (20). The amplitude $C = C(\tau)$ is introduced since the magnitude of an eigenvector is arbitrary. The amplitude C is determined during the solution process for the third-order equations.

(2) *Second order* (ε^2). Since the differential operator defining the left-hand side of the second-order equations, Eq. (28), is the same as that for the first-order equations, we may write the discretized form of the second-order equations as

$$\boldsymbol{\alpha}\mathbf{x}_{(2)} = \mathbf{f}_{(2)} \tag{37}$$

where

$$\mathbf{x}_{(2)} = \left(\psi^{(2)}_{3,3}, \psi^{(2)}_{4,3}, \ldots, \psi^{(2)}_{NX-1,NY-1}, \Theta^{(2)}_{2,2}, \Theta^{(2)}_{3,2}, \ldots, \Theta^{(2)}_{NX,NY}\right)^{\mathrm{T}} \tag{38}$$

and $\mathbf{f}_{(2)}$ is determined by the right-hand side of Eq. (28).

Eq. (38) can be easily solved to yield $\mathbf{x}_{(2)}$.

(3) *Third order* (ε^3). The third order equations, Eq. (29), may be discretized as

$$\boldsymbol{\alpha}\mathbf{x}_{(3)} = \frac{\partial}{\partial\tau}\mathbf{f}_{(3)} + R_2 Pr\,\mathbf{g}_{(3)} + \mathbf{h}_{(3)} \tag{39}$$

where $\boldsymbol{\alpha}$ is the same matrix as defined previously and $\mathbf{x}_{(3)}$ is given by

$$\mathbf{x}_{(3)} = \left(\psi^{(3)}_{3,3}, \psi^{(3)}_{4,3}, \ldots, \psi^{(3)}_{NX-1,NY-1}, \Theta^{(3)}_{2,2}, \Theta^{(3)}_{3,2}, \ldots, \Theta^{(3)}_{NX,NY}\right)^{\mathrm{T}} \tag{40}$$

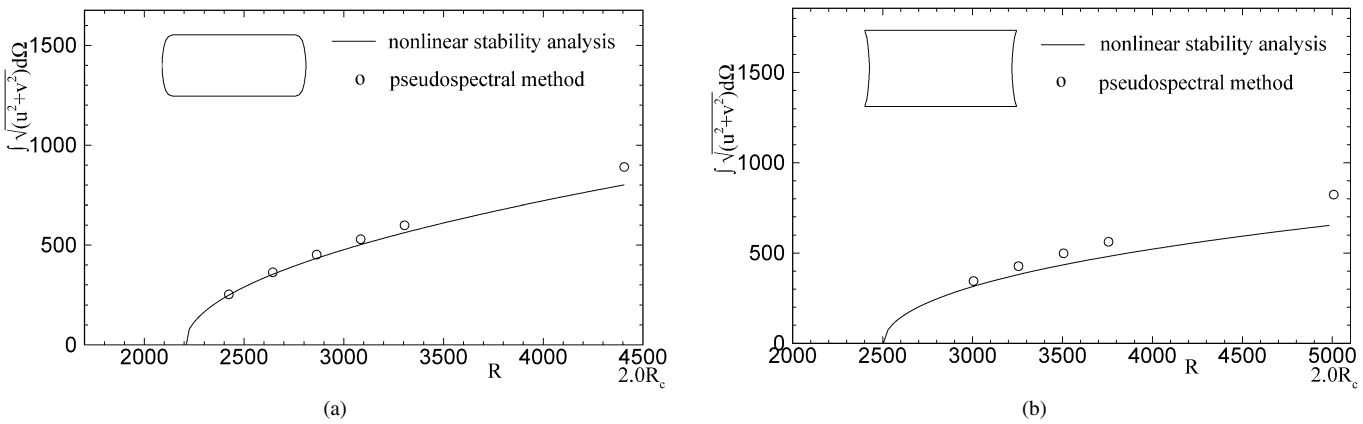

Fig. 7. Intensity of convection versus the Rayleigh number: comparison of the nonlinear stability analysis and the Chebyshev pseudospectral simulation for each of the two shapes depicted in the figures.

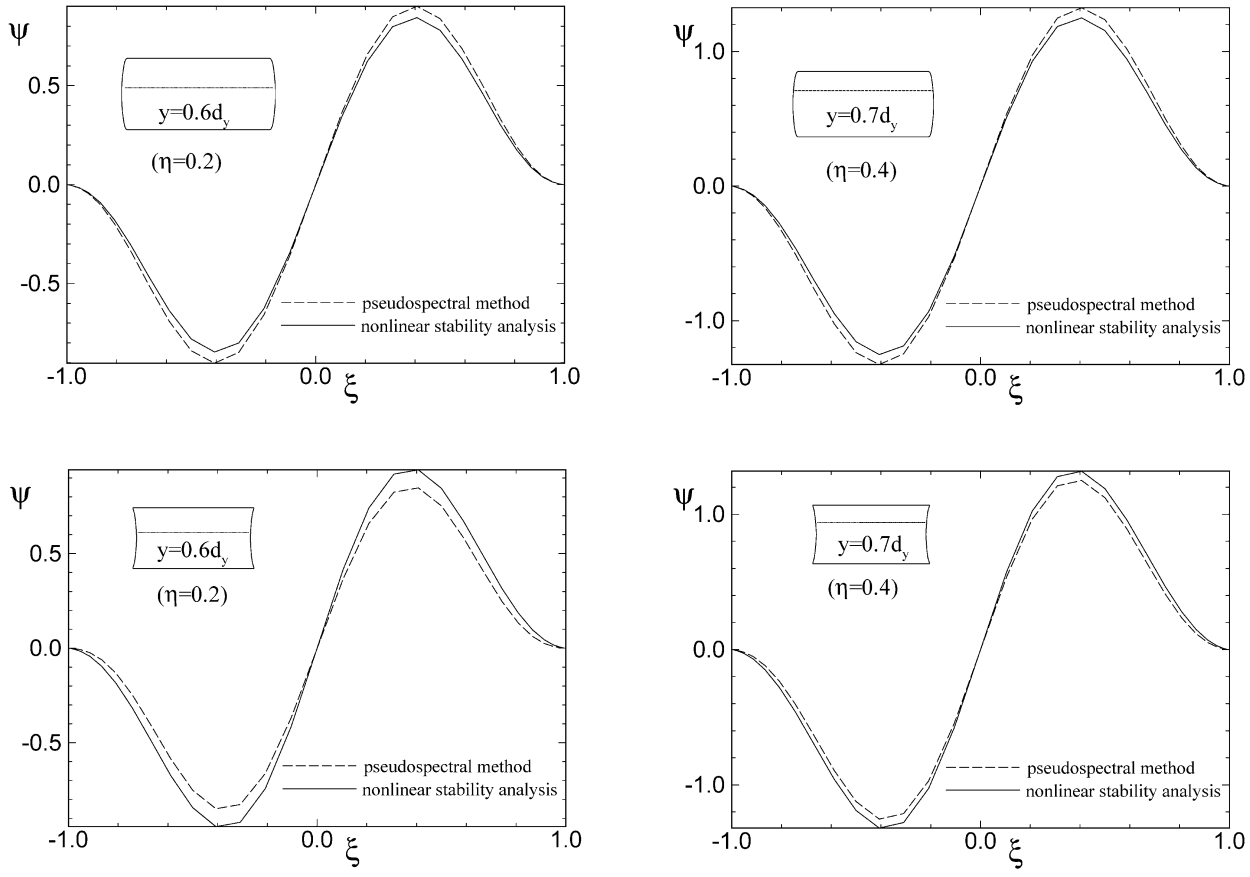

Fig. 8. Comparison of the nonlinear stability analysis and pseudospectral simulation; stream function ψ.

The vectors $\mathbf{f}_{(3)}$,$\mathbf{g}_{(3)}$, and $\mathbf{h}_{(3)}$ are determined using the right-hand side of Eq. (29).

Since the vector $\mathbf{h}_{(3)}$ consists of terms which are multiples of the first-order solution and the second-order solution, it is proportional to C^3.

(4) *Adjoint problem*. The adjoint equation to the linear stability problem, Eq. (21), is given by

$$\left(\boldsymbol{\beta}^{-1}\cdot\boldsymbol{\alpha}\right)^{\mathrm{T}}\cdot\mathbf{y}=-s\mathbf{y} \tag{41}$$

where the superscript T denotes the matrix transpose. The eigenvector $\mathbf{y}$ with zero eigenvalue ($s=0$) is the adjoint solution of the linear stability problem.

The Landau equation that describes the temporal variation of the amplitude C of the convection cell is derived as follows. Multiplying both sides of Eq. (40) by $\boldsymbol{\beta}^{-1}$, where $\boldsymbol{\beta}$ is defined in Eq. (21), and taking inner product of the resulting equation with the adjoint vector $\mathbf{y}$, we find

$$\left\langle\mathbf{y},\left(\boldsymbol{\beta}^{-1}\cdot\boldsymbol{\alpha}\right)\cdot\mathbf{x}_{(3)}\right\rangle=\frac{\partial}{\partial\tau}\left\langle\mathbf{y},\boldsymbol{\beta}^{-1}\cdot\mathbf{f}_{(3)}\right\rangle+R_2\,Pr\left\langle\mathbf{y},\boldsymbol{\beta}^{-1}\cdot\mathbf{g}_{(3)}\right\rangle+\left\langle\mathbf{y},\boldsymbol{\beta}^{-1}\cdot\mathbf{h}_{(3)}\right\rangle \tag{42}$$

Since the left-hand side of Eq. (42) is zero from the definition of the adjoint solution, we find the following form of the Landau equation:

$$\left\langle \mathbf{y}, \boldsymbol{\beta}^{-1} \cdot \mathbf{F}_{(3)} \right\rangle \frac{\partial C}{\partial \tau} + R_2 Pr\, C \left\langle \mathbf{y}, \boldsymbol{\beta}^{-1} \cdot \mathbf{G}_{(3)} \right\rangle + C^3 \left\langle \mathbf{y}, \boldsymbol{\beta}^{-1} \cdot \mathbf{H}_{(3)} \right\rangle = 0 \tag{43}$$

For the supercritical bifurcation, which is the usual case with the normal Rayleigh–Bénard problem, we can find the steady amplitude of the convection cell from Eq. (43) as

$$\varepsilon C_s = \sqrt{\frac{-(R - R_c)\langle \mathbf{y}, \boldsymbol{\beta}^{-1} \cdot \mathbf{G}_{(3)} \rangle}{\langle \mathbf{y}, \boldsymbol{\beta}^{-1} \cdot \mathbf{H}_{(3)} \rangle}} \tag{44}$$

where Eq. (22) is invoked to replace R_2 in terms of R and R_c. From this, we can obtain the velocity and temperature field at the steady state for a given Rayleigh number exploiting Eqs. (23)–(24).

To corroborate the results of the nonlinear stability analysis, we solve the Navier–Stokes equation using the Chebyshev pseudospectral method and compare the results with those of the nonlinear stability analysis. Details of the Chebyshev pseudospectral method as applied to the Boussinesq equation are given in Park and Chung [17]. Figs. 7(a) and 7(b) show the intensity of convection, defined as the magnitude of velocity integrated over the domain, versus the Rayleigh number for the two domains depicted in the same figure. The solid line denotes the convection intensity obtained by the nonlinear stability analysis, while that from the pseudospectral method is indicated by small circles. It is shown that the nonlinear stability analysis predicts correct convection intensity even when the Rayleigh number R is over $1.5R_c$.

Fig. 8 shows the comparison of the stream function ψ obtained by the nonlinear stability analysis and pseudospectral simulation, respectively, for the two domains shown in Fig. 7. This result corroborate the pointwise coincidence between the results of the nonlinear stability analysis and those of the pseudospectral simulation.

6. Conclusion

A method is suggested for the linear and nonlinear stability analysis of the Rayleigh–Bénard convection in arbitrary finite domains. Employing this technique, the effects of the sidewall distortion on the critical Rayleigh number have been investigated. Also investigated is the difference in the switching pattern of cell numbers as the aspect ratio varies, between the isothermal sidewalls and the adiabatic sidewalls. The present technique allows us to derive a Landau equation that predicts the evolution of the convection cell in arbitrary finite domains. The results based on the nonlinear stability analysis are compared with those obtained from the numerical solution of the Navier–Stokes equation with the Boussinesq approximation, and both results are found to be in good agreement with each other. The present work shows the possibility of controlling thermal convection by varying the shape of the convection domain. It is also shown that the nonlinear stability analysis is an economical alternative way of obtaining convection pattern to the direct numerical simulation near the critical Rayleigh number.

Acknowledgements

This work was supported by grant No. R01-2003-000-10224-0 from Korea Science and Engineering Foundation.

References

[1] S. Chandrasekhar, Hydrodynamic and Hydromagnetic Stability, Oxford University Press, London, 1961.
[2] P.G. Drazin, W.H. Reid, Hydrodynamic Stability, Cambridge University Press, Cambridge, 1981.
[3] W.V.R. Malkus, G. Veronis, Finite amplitude cellular convection, J. Fluid Mech. 4 (1958) 225–260.
[4] A. Schlüter, D. Lortz, F. Busse, On the stability of steady finite amplitude convection, J. Fluid Mech. 23 (1965) 129–144.
[5] S.H. Davis, Convection in a box: Linear theory, J. Fluid Mech. 30 (1967) 465–478.
[6] B.D. Reddy, H.F. Voyè, Finite element analysis of the stability of fluid motions, J. Comput. Phys. 79 (1988) 92.
[7] A.I. van de Vooren, H.A. Dijkstra, A finite element stability analysis for the Marangoni problem in a rectangular container with rigid sidewalls, Comput. Fluids 17 (1989) 467.
[8] G.S. Charlson, R.L. Sani, Finite amplitude axisymmetric thermoconvective flows in a bounded cylindrical layer of fluid, J. Fluid Mech. 71 (1975) 209–230.
[9] E. Crespo del Arco, P. Bontoux, Numerical solution and analysis of asymmetric convection in a vertical cylinder: An effect of Prandtl number, Phys. Fluids A 1 (1989) 1348–1359.
[10] H.M. Park, D.H. Ryu, A solution method of nonlinear convective stability problems in finite domains, J. Comput. Phys. 170 (2001) 141.
[11] L.A. Segel, Distant sidewalls cause slow amplitude modulation of cellular convection, J. Fluid Mech. 38 (1969) 203–224.
[12] P.G. Daniels, The effect of distant sidewalls on the transition to finite amplitude Bénard convection, Proc. Roy. Soc. London A 358 (1977) 199–221.
[13] M.C. Cross, P.C. Hohenberg, Pattern formation outside of equilibrium, Rev. Modern Phys. 65 (1993) 851.
[14] G.R. Hardin, R.L. Sani, Buoyancy-driven instability in a vertical cylinder: binary fluids with Soret effect, Part II: Weakly nonlinear solutions, Int. J. Methods Engrg. 17 (1993) 755–786.
[15] R. Peyret, Spectral Methods for Incompressible Viscous Flow, Springer, Berlin, 2002.
[16] J.F. Thompson, Z.U.A. Warsi, Numerical Grid Generation, North-Holland, Amsterdam, 1985.
[17] H.M. Park, O.Y. Chung, Inverse natural convection problem of estimating wall heat flux using a moving sensor, ASME J. Heat Transfer 121 (1999) 828.